Journal of
Composites Science

MDPI

Article

Experimental and Statistical Modeling for Effect of Nozzle Diameter, Filling Pattern, and Layer Height of FDM-Printed Ceramic–Polymer Green Body on Biaxial Flexural Strength of Sintered Alumina Ceramic

Anton Smirnov [1,*], Nikita Nikitin [2,*], Pavel Peretyagin [2,3], Roman Khmyrov [4], Ekaterina Kuznetsova [1] and Nestor Washington Solis Pinargote [1,2]

[1] Laboratory of 3D Structural and Functional Engineering, Moscow State University of Technology "STANKIN", Vadkovsky per. 1, Moscow 127055, Russia; e.kuznetsova@stankin.ru (E.K.); nw.solis@stankin.ru (N.W.S.P.)
[2] Spark Plasma Sintering Research Laboratory, Moscow State University of Technology "STANKIN", Vadkovsky per. 1, Moscow 127055, Russia; p.peretyagin@stankin.ru
[3] Scientific Department, A.I. Evdokimov Moscow State University of Medicine and Dentistry, Delegatskaya St., 20, p.1, Moscow 127473, Russia
[4] Laboratory of Innovative Additive Technologies, Moscow State University of Technology "STANKIN", Vadkovsky per. 1, Moscow 127055, Russia; r.khmyrov@stankin.ru
* Correspondence: a.smirnov@stankin.ru (A.S.); nikitin5@yandex.ru (N.N.); Tel.: +7-4999-7323-70 (A.S. & N.N.)

Abstract: This paper deals with the application of statistical analysis in the study of the dependence of the flexural strength of sintered alumina (Al_2O_3) disks on the parameters (nozzle diameter of the printer print head, layer height, and filling pattern) of the fused deposition method (FDM) printing of ceramic–polymer filament containing 60 vol.% alumina and 40 vol.% polylactide. By means of a correlation analysis applied to the results of flexural tests, a linear relationship was found between the thickness of the printed layer and the strength of the sintered specimens. A statistically significant linear relationship was found between the geometric parameters and the weight of both printed ceramic–polymer and sintered ceramic samples, as well as the diameter of the nozzle used in the printing of the workpiece. It was found that the highest strength is achieved with a layer thickness equal to 0.4 mm, and the smallest scatter of mass values and geometric dimensions of ceramic samples is achieved using a nozzle diameter of 0.6 mm. As a result of the conducted research, linear equations allowing the prediction of changes in the geometry and mass of samples after sintering, as well as the strength properties of sintered samples, taking into account the geometry and mass of FDMed samples, were obtained.

Keywords: additive manufacturing; fused deposition modeling; ceramic–polymer filament; statistical analysis; biaxial strength

Citation: Smirnov, A.; Nikitin, N.; Peretyagin, P.; Khmyrov, R.; Kuznetsova, E.; Solis Pinargote, N.W. Experimental and Statistical Modeling for Effect of Nozzle Diameter, Filling Pattern, and Layer Height of FDM-Printed Ceramic–Polymer Green Body on Biaxial Flexural Strength of Sintered Alumina Ceramic. *J. Compos. Sci.* **2023**, *7*, 381. https://doi.org/10.3390/jcs7090381

Academic Editors: Francesco Tornabene and Thanasis Triantafillou

Received: 10 August 2023
Revised: 3 September 2023
Accepted: 7 September 2023
Published: 12 September 2023
Corrected: 4 March 2024

1. Introduction

Aluminum oxide (Al_2O_3) has useful properties such as a high melting point, hardness, and wear and chemical resistance [1–4]. It can be used in refractories, electrical insulators, wear-resistant mechanism parts, artificial jewelry, abrasive material, ceramic armor parts, etc. Among others, Al_2O_3 is used in medicine for dental and orthopedic implants [5–7]. However, on the other hand, the high hardness and brittleness of ceramic materials also make it difficult for shaping and machining. Methods such as slurry casting, dry pressing, and plastic molding have certain disadvantages [8–11]: forming complex components requires the use of molds with high geometric accuracy. Because high-precision molds are costly to manufacture and have long production runs, it is difficult to continuously improve and upgrade the product; sintered samples often require either laser processing or

machining using diamond cutting tools to ensure sufficient accuracy in the dimensions and shape of the finished product; some special shapes and elements are difficult to produce using conventional molding processes, such as internal cavities, holes, and internal grooves. These disadvantages have placed significant limitations on the widespread use of ceramic products. By using additive manufacturing technologies to form complex ceramic parts, it is possible to circumvent the aforementioned problems, reduce scrap rates, increase production flexibility, and enable rapid production of ceramic parts with complex shapes. According to the International Organization for Standardization (ISO), together with the American Society for Testing and Materials (ISO/ASTM 52900:2015) [12], these technologies are classified into groups, among which the most widely used 3D printing process is material extrusion, which includes layer-by-layer fused deposition modeling (FDM). The main advantage of this technology is the availability and simplicity of equipment, as well as the ability to quickly create prototypes with complex geometry. In FDM, an object is built by depositing molten material over a pre-created digital model (CAD) layer by layer. The materials most commonly used are thermoplastic polymers in the form of filament wound on a spool. However, recently, there has been a steady interest in the use of this technology for printing ceramic products where highly filled (>50 vol.%) ceramic–polymer filaments are used as feedstock. For example, Tosto et al. reported a sintered α-alumina with a mean density, tensile strength, and Vickers hardness of 3.80 g/cm^3, 232.6 $\pm$ 12.3 MPa, and 21 $\pm$ 0.7 GPa, respectively, was derived from commercially available alumina/polymer filament using fused filament fabrication (FFF) method [13]. Nötzel et al. developed a 60 vol.% alumina-low density polyethylene as filament material that can be printed on a low-cost FFF. Post-processed ceramic discs showed 97.3% of theoretical density [14]. Iyer et al. reported on the methods for the fabrication and results of using FDM to produce silicon nitride samples from manufactured filament feedstock with 55 vol.% of investment casting wax as a binder. Obtained dense (>99%) sintered ceramic parts exhibited microstructure and mechanical (strength 908 MPa, fracture toughness 8.53 MPa·m$^{1/2}$) characteristics similar to conventionally manufactured samples [15]. Orlovská et al. used a composite filament containing 50 vol.% of sub-micron alumina powder for FFF and subsequent sintering. Produced parts demonstrated relative densities ranging from 80 to 89%, and the flexural strength reached 200–300 MPa depending on the layer thickness used for the printing [16]. Truxová et al. presented a comprehensive study of the processing and mechanical properties of the ceramic material Al_2O_3 on FFF. After debinding and sintering the alumina (52 vol.%)—thermoplastic printed samples—a density of 99.72%, a maximum hardness of 23.81 GPa, and a flexural strength of 331.61 MPa were obtained [17]. Schätzlein et al. highlighted that the use of the filament consists of biodegradable polylactide acid and a varying amount (up to 20%) of osteoconductive S53P4 bioglass for scaffolds with optimized physico-mechanical and biological properties [18]. Elhattab et al. developed 3D-printable β-Tricalcium Phosphate–PLA composite filaments. The manufactured filaments had a constant diameter and uniform distribution of ceramic particles inside the polymer matrix and were effectively used for 3D printing parts via the FDM method, considering the specifics of the design and mechanical properties, which are widely used in orthopedics and dental biomedicine [19]. Tselikos et al. presented a conceptual design on how to use an alternating electric field to simultaneously 3D-print a polylactic acid $K_{0.485}Na_{0.485}La_{0.03}NbO_3$ composite with aligned ceramic particles using a solvent-free FFF technique [20]. Nakonieczny et al. created polyamide-30 wt.% ceramic (alumina or zirconia) filaments for 3D FDM printing. It was found that mechanical properties depend on the printing temperature; filler use slightly reduced the tensile strength and Young's modulus of bare polyamide [21]. Changing the type of filler, its volume content, particle size, and shape of particles leads to changes in the strength properties of the final objects [22,23]. These characteristics depend on many factors (equipment and printing parameters, heat treatment modes, etc.), which should be considered together, not separately [24–26]. For this purpose, it is possible to use full-scale experiments that are as close to practice as possible. However, such studies are too expensive and

energy-consuming. Therefore, the use of mathematical apparatus to determine the behavior of the object, taking into account external influences, is a good alternative to replacing the real system with an appropriate model [27,28]. For instance, Fountas et al. examined the influence of nozzle temperature and layer thickness on the ultimate tensile strength and modulus of elasticity of PLA and PLA-based composites using statistical analysis. At the same time, a regression analysis followed to generate full quadratic equations that would correlate the independent variables with the objectives. The regression models (full quadratic equations) were implemented as objective functions to be iteratively evaluated by the grey-wolf algorithm, aiming at maximizing both responses simultaneously [29]. Banerjee et al. investigated various FDM process parameters on the performance of the printed parts using a design of experiment approach, i.e., the response surface methodology technique was adopted to generate maximum data from a smaller number of experimental running orders. A method has been developed for predicting the roughness of FDM samples, which can affect mechanical strength, geometric accuracy, and surface cleanliness [30]. Fountas et al. focused on the influence of the FDM modeling parameters on the specimen's tensile strength. In order to find optimal parameter settings using any artificial intelligent algorithm or neural network, a regression model can be applied that adequately explains the variations and non-linear influence of FDM parameters on the tensile strength [31]. Crockett has investigated the deposition and liquid-to-solid transition phase of the FDM process by developing an analytical model for bead spreading [32]. Anitha et al. focused on optimizing the FDM process surface quality [33]. Taking into consideration Taguchi's analysis, three variables have been investigated, which are the road width, build layer thickness, and speed of deposition. In addition, analysis of variance has been performed with the same parameters. Bellini et al. and Venkataraman et al. have analytically modeled the material flow on the extrusion nozzle [34,35]. Venkataraman et al. predicted the performance of the lead zirconate titanate (52.6 vol.%)—polymer material in the FDM as a function of nozzle geometry and volumetric flow rate based on the quantity extrusion pressure/compressive modulus [36]. It should be noted that in a number of cases [27,37–39], no proper attention is paid to analyzing whether the data obtained from tensile tests belong to the normal distribution; the analysis is carried out either by graphical methods [38] or it is claimed that the data distribution belongs to the normal distribution [27,37,38]. The authors [40] note that in the case of a weak variation in the effect under study, the choice of the statistical analysis method, depending on the law of distribution to which the data in the study obey, practically does not affect the conclusions and the magnitude of the effect drawn from the results of the analysis, but in the problems of materials science, the variation in the mechanical characteristics of the material can be quite high [41] and requires close attention to the statistical methods used in the analysis of research results. In order to assess the strength values, a biaxial bending test was used according to the ISO 6872:2019 method [42]. For this technique, the requirements for the preparation and shape of samples are not as strict as compared to conventional bending tests at three or four points [43–46]. In this paper, the statistical analysis of biaxial flexural test results of sintered ceramic specimens produced by the FDM method with debinding–sintering processes from a fabricated ceramic–polymer filament filled with alumina (60 vol%) particles and establish a statistical relationship between the 3D printer nozzle diameter, layer height, and filling pattern on the strength characteristics of these specimens.

2. Materials and Methods

2.1. Fabrication of Ceramic–Polymer Filament

The ceramic–polymer filament containing (by volume) 60% wear-resistant, biocompatible, high-hardness material, namely α-aluminum oxide (Al_2O_3, Plasmotherm Ltd., Moscow, Russia) and 40% polylactide (PLA, eSun Ltd., Shenzhen, China) was wet mixed in an ML-1C (Promstroimash, Kaluga, Russia) ball mill for 24 h from corresponding portions of ceramic and PLA. The obtained suspension was dried in a vacuum desiccator for

24 h at 90 °C and then sieved on a vibratory sieve shaker. Details of the ceramic/polymer suspension processing were reported elsewhere [47].

2.2. Printing, Debinding and Sintering

The ceramic–polymer filament was produced at 220 °C and with a nozzle diameter of 1.7 ± 0.1 mm using a Wellzoom desktop extruder (Wellzoom, Shanghai, China). Printing of samples from experimental ceramic–polymer filaments was carried out on a Black Widow 3D printer (Tevo 3D, Zhanjiang, China) using the PrusaSlicer 2.5.2. software. The printing parameters selected for optimization were as follows: layer height (0.2, 0.3, 0.4 mm), nozzle diameter (0.6, 0.8, 1.0 mm), and filling pattern (zigzag, concentric, line). The filling percentage during printing was equal to 100%, regardless of the other parameters. The thermal debinding (up to 600 °C) and sintering (1550 °C) were conducted on printed "green" specimens in SNOL 1.7/1700 (AB Umega, Utena, Lithuania) air furnace. Detailed description of these processes is available in previous work [47].

2.3. Physical and Mechanical Characterization

In order to determine the true density of the initial aluminum oxide powder, an AccuPyc 1340 (Micromeritics, Norcross, GA, USA) helium automatic pycnometer was used. The density of sintered compacts was determined by the Archimedes method in distilled water. The samples were weighed in air and in a liquid medium on electronic balance with an accuracy of 0.0001 g. The flexural strength of sintered disk-shaped ceramic samples was determined by a biaxial bending test according to the ISO 6872:2019 method [42]. The central part of the sample was subjected to uniform biaxial stress. Each sintered and polished sample was placed in the center on three hardened steel balls (with a diameter of 3 mm, located at an angle of 120° to each other on a support circle with a diameter of 10 mm). The surface of the sample was loaded with a flat pin with a diameter of 1.6 mm in the center of the sample with a traverse movement speed of 1 mm/min until failure. The load (N) after the specimen was broken was recorded, and the strength was calculated. All mechanical tests were performed at room temperature with a testing machine Electropuls E10000 (Instron, Norwood, MA, USA). Details of the calculation procedures were reported elsewhere [44]. Statistical analysis of the results of the experiment was carried out using software (Rstudio 2023.06.1 Posit Software, PBC, GNU license) written in the R language.

3. Results and Discussion

Figure 1 presents optical images of 3D-printed disk-shaped ceramic–polymer samples with different filling patterns, layer height, and nozzle diameter.

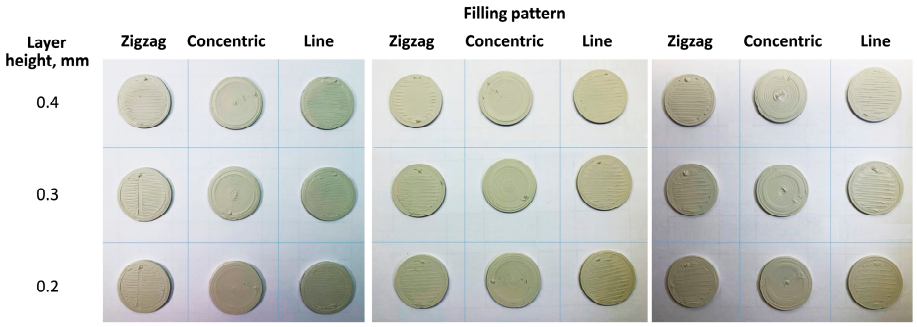

Figure 1. FDM printed specimens with different fill patterns, layer height and nozzle (left 0.6 mm, center 0.8 mm, right 1 mm) diameter.

After visual inspection of the ceramic–polymer disks, no obvious defects were found on the surface. Therefore, all samples were subjected to burning out the polymer binder and sintering to obtain ceramic specimens. After debinding and sintering, the specimens reached 93 % of the true density (3.95 g/cm^3) of alumina powder, which is equivalent to a porosity of 7 %. The water absorption of sintered alumina was 109 %. Table 1 shows the

geometrical parameters of the printed and sintered specimens and the results of calculating the biaxial flexural strength of sintered specimens.

Table 1. Weight (w), diameter (d), thickness (h), and strength (σ_H) of 3D-printed and sintered $60Al_2O_3/40PLA$ samples as a function of selected FDM printing parameters.

№	Nozzle Diameter, mm	Layer Height, mm	Filling Pattern	Samples						σ_H, MPa
				Printed			Sintered			
				w, g	d, mm	h, mm	W, g	D, mm	H, mm	
1	0.6	0.2	Zigzag	2.7	25.9	2.2	2.3	21.6	1.6	242
2		0.3		2.5	25.9	1.9	2.1	22.3	1.6	245
3		0.4		2.8	25.8	2.3	2.5	22.2	2.1	268
4		0.2	Line	2.7	25.9	2.3	2.3	22.4	1.6	277
5		0.3		2.5	25.5	2.1	2.2	21.9	1.7	315
6		0.4		2.8	25.7	2.2	2.3	21.9	1.9	332
7		0.2	Concentric	2.6	25.9	2.0	2.2	22.3	1.6	228
8		0.3		2.4	25.6	1.9	2.0	22.0	1.6	236
9		0.4		2.7	25.8	2.1	2.3	21.8	1.8	248
10	0.8	0.2	Zigzag	2.7	25.4	2.0	2.3	22.1	1.7	215
11		0.3		2.5	25.4	1.9	2.1	21.9	1.6	260
12		0.4		2.5	25.3	1.9	2.2	21.5	1.6	265
13		0.2	Line	2.7	25.8	2.2	2.3	21.1	2.0	280
14		0.3		2.5	25.7	2.0	2.1	21.8	1.7	292
15		0.4		2.5	24.8	2.0	2.2	21.0	1.8	322
16		0.2	Concentric	2.7	25.6	2.0	2.3	22.0	1.9	191
17		0.3		2.5	25.5	1.9	2.1	22.0	1.7	196
18		0.4		2.8	25.4	2.0	2.0	21.3	1.7	250
19	1.0	0.2	Zigzag	2.8	26.1	2.3	2.4	22.5	1.9	275
20		0.3		2.6	25.3	2.1	2.1	21.9	1.7	280
21		0.4		2.8	25.1	2.3	2.4	21.3	1.9	295
22		0.2	Line	2.8	25.2	2.2	2.4	21.5	2.0	277
23		0.3		2.8	25.2	2.3	2.4	21.9	2.0	298
24		0.4		3.2	25.4	2.4	2.7	21.9	2.0	327
25		0.2	Concentric	2.9	25.3	2.3	2.5	21.5	1.9	180
26		0.3		2.9	25.2	2.3	2.6	21.7	2.0	203
27		0.4		2.7	25.5	2.2	2.3	21.8	1.9	230

Statistical analysis methods were used to establish the relationship between the geometric characteristics of the printed and sintered specimens, as well as the printing parameters and the calculated strength values. Table 2 summarizes the results of the basic statistical analysis of the change in the geometry of the printed green bodies after sintering and the values of flexural strength.

The results show that the greatest spread in percentage terms is achieved in the change in the height of sintered samples in relation to the printed ones. This correlates with the previously mentioned fact, according to which the shrinkage along the Z axis of printed samples is higher than in the radial direction [13,48]. In absolute terms, the samples obtained by the presented technology have a high variation in mechanical properties under biaxial loading. Further study of the data by statistical methods of analysis is based on the choice of criterion, by which the belonging of the distribution of the studied random variable to the normal distribution is checked. Currently, there are more than 40 [49] different criteria. In this paper, we consider two criteria—the Shapiro–Wilk criterion [50] and the Kolmogorov–Smirnov criterion [51]. These two criteria were compared by the Monte Carlo simulation method based on the calculation of the average power of the criterion as a function of the number of trials. As input data for the criterion, six distribution laws were

set, the parameters of which were calculated by the maximum likelihood method [52,53]: normal, log-normal, logarithmic normal, logistic, Weibull, Cauchy, and exponential. Each of the distributions was substituted into the criterion under study, and based on the results of 100,000 repetitions, the average power of the criterion was calculated as a function of the number of studies. Figure 2 shows the results of the Monte Carlo simulation of the dependence of the average criterion power on the number of studies.

Table 2. The results of basic statistical analysis of the selected studied parameters are presented in Table 1.

Value	Weight Change, %	Diameter Change, %	Height Change, %	σ_H, MPa
Mean	15.35	14.55	15.45	260.1
Median	14.81	14.06	15.79	265.0
Maximum	28.57	18.22	30.43	332.0
Minimum	10.71	12.99	5.00	180.0
Mean square deviation	3.20	1.15	5.31	41.78

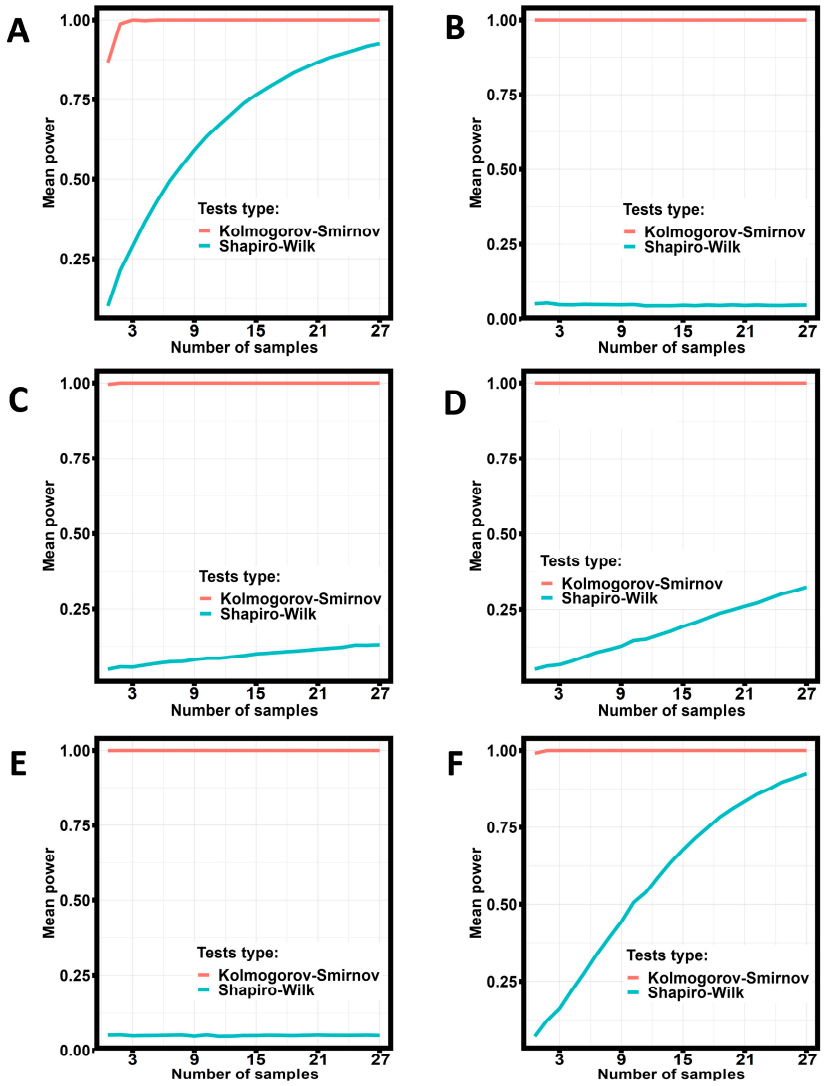

Figure 2. Results of Monte Carlo simulation of the power of statistical criteria as a function of the number of studies in the study sample for the Cauchy (**A**), Weibull (**B**), logistic (**C**), log-normal (**D**), normal (**E**), and exponential (**F**) distribution.

The presented simulation results show that the Kolmogorov–Smirnov test has the maximum power, and the average power of this criterion does not depend on what distribution law the analyzed data obey, i.e., it has the lowest probability of committing an error of the second kind. It should be noted that the Kolmogorov–Smirnov test reaches the maximum power close to one when the number of tests is greater than or equal to five. The exception is the case where the data obey the exponential distribution law (Figure 2F), in which case the average power of the Kolmogorov–Smirnov and Shapiro–Wilk tests practically coincide. Table 3 presents the results of applying the Kolmogorov–Smirnov test to the geometry of printed and sintered samples and the strength properties presented in Table 1. As a null hypothesis, it is accepted that the data belong to the distribution not different from normal, with a level of statistical significance of p-value = 0.05 (this level of statistical significance is used for all used statistical criteria).

Table 3. Results of applying Kolmogorov–Smirnov test to the data under study.

	Printed			Sintered			σ_H
	w	**d**	**h**	**W**	**D**	**H**	
D value of Kolmogorov–Smirnov test	0.992	1	0.971	0.977	1	0.945	1
Level of statistical significance, p-value ($\times 10^{-16}$)	2.2	2.2	2.2	2.2	2.2	2.2	2.2

The results of applying the Kolmogorov–Smirnov criterion to the experimental results obtained show that the data are distributed differently from the normal distribution (p-value << 0.05) with a high maximum divergence of data distribution functions from the normal distribution (D $\rightarrow$ 1) and all further statistical studies should be carried out by nonparametric methods [54]. In order to identify the linear relationship between printing parameters, printed and sintered geometry, and strength values, the Spearman correlation matrix was calculated, and the power of correlation was interpreted using the Evans scale. The results of the calculations are presented in Table 4.

Table 4. Spearman correlation coefficient matrix for the values presented in Table 1.

		Nozzle Diameter	Layer Height	σ_H	Printed			Sintered		
					w *	d *	h *	W *	D*	H *
	Nozzle diameter	1	0	0.050	0.485	−0.641	0.407	0.428	0.346	0.536
	Layer height		1	0.382	0.014	−0.316	−0.033	−0.086	−0.302	0.143
	σ_H			1	0.073	0.158	0.307	0.081	0.203	0.237
printed	w				1	0.183	0.837	0.833	0.157	0.738
	d					1	−0.063	−0.147	0.584	0.301
	h						1	0.871	0.075	0.693
sintered	W							1	−0.067	0.764
	D								1	−0.274
	H									1

* w—weight; d—diameter; h—height.

From the results of calculating the Spearman correlation coefficients, it follows that there is no correlation between the nozzle diameter and strength value, the height and diameter of the printed samples, the height of the printed and diameter of the sintered samples, the weight of the sintered sample and strength value, the layer height and weight of the printed sample, the layer and printed sample height, the layer height of the printed and weight and strength value of the sintered samples, the diameter of the sintered and height and weight of the printed samples. The strongest correlation (0.871) was found between the height of the printed samples and the weight of the sintered samples. In

other cases, a correlation of different strengths was observed, which should be checked for statistical significance. Table 5 summarizes the results of correlation verification for statistical significance level for the flexural strength values of sintered alumina specimens.

Table 5. Verification results of the statistical significance of Spearman correlation coefficients.

		Correlated Pairs						
		Statistical Significance Level of Correlation *p*-Value						
				Printed			***Sintered***	
		Layer Height	**Nozzle Diameter**	***d***	***h***	***W***	***D***	***H***
	σ_H	0.05 (according to Kendall 0.04)		0.4303	0.1199	0.6864	0.3109	0.2333
printed	*w*		0.0100	0.3592	$5.2 \cdot 10^{-8}$	$6.76 \cdot 10^{-8}$	0.4352	$1.094 \cdot 10^{-5}$
printed	*d*	0.1079	0.0003				0.001	0.1269
printed	*h*		0.0350			$3.466 \cdot 10^{-9}$	0.7086	$6.228 \cdot 10^{-5}$
sintered	*W*	0.6693	0.0260					$3.583 \cdot 10^{-6}$
sintered	*D*	0.1255	0.0770					0.2138
sintered	*H*	0.4767	0.0040					

Kendall's correlation was also used to refine correlation coefficient values in controversial moments (close to 0.05). As a result of the analysis, the flexural strength of the specimens was found to be linearly dependent on the height of the layer (p-value < 0.05). The diameter of the printer nozzle is statistically significantly correlated with all geometric parameters of printed and sintered samples, except for the diameter of the ceramic specimens. At the same time, the diameter of the green bodies is statistically significantly correlated with the diameter of the alumina samples. The correlation between the height of the layer and the FDMed and Al_2O_3 specimens' geometry, as well as between their weight, is not statistically significant (p-value > 0.05). In order to determine the degree of influence of one statistically significantly correlated parameter on another, the coefficients of determination were calculated and presented in Table 6. In this table, the larger the value of the coefficient of determination, the more strongly one parameter affects the other.

Table 6. Determination coefficients of statistically significantly correlated parameters.

Correlating Parameters		**Determination Coefficient, %**
σ_H—Layer height		14.56
Nozzle diameter	- w *	23.46
	- d *	41.14
	- W	18.29
	- H	28.76
d *—*D*		34.08

* for printed samples.

The obtained statistically significant correlations allow us to state that it is recommended to use a nozzle with a diameter as small as possible when printing samples from fabricated ceramic–polymer filament using FDM technology. The use of a nozzle with a

minimum diameter leads to an insignificant scattering of geometric parameters (in particular, diameter) of both printed and sintered samples. The high correlation values between the geometrical characteristics of the printed and sintered samples indicate a negligible change in the diameter and height of the Al_2O_3 specimens. The presence of a weak linear statistically significant relationship between the flexural strength of ceramic specimens and the layer thickness shows that an increase in the height of the flayer leads to an increase in the strength of the specimen by 14.56%. The choice of technological elements, in particular nozzle diameter, depending on the geometry of the printed objects, is of practical importance in the design and manufacture of finished products. Figure 3 presents scatter diagrams and robust linear regression equations for the identified correlations.

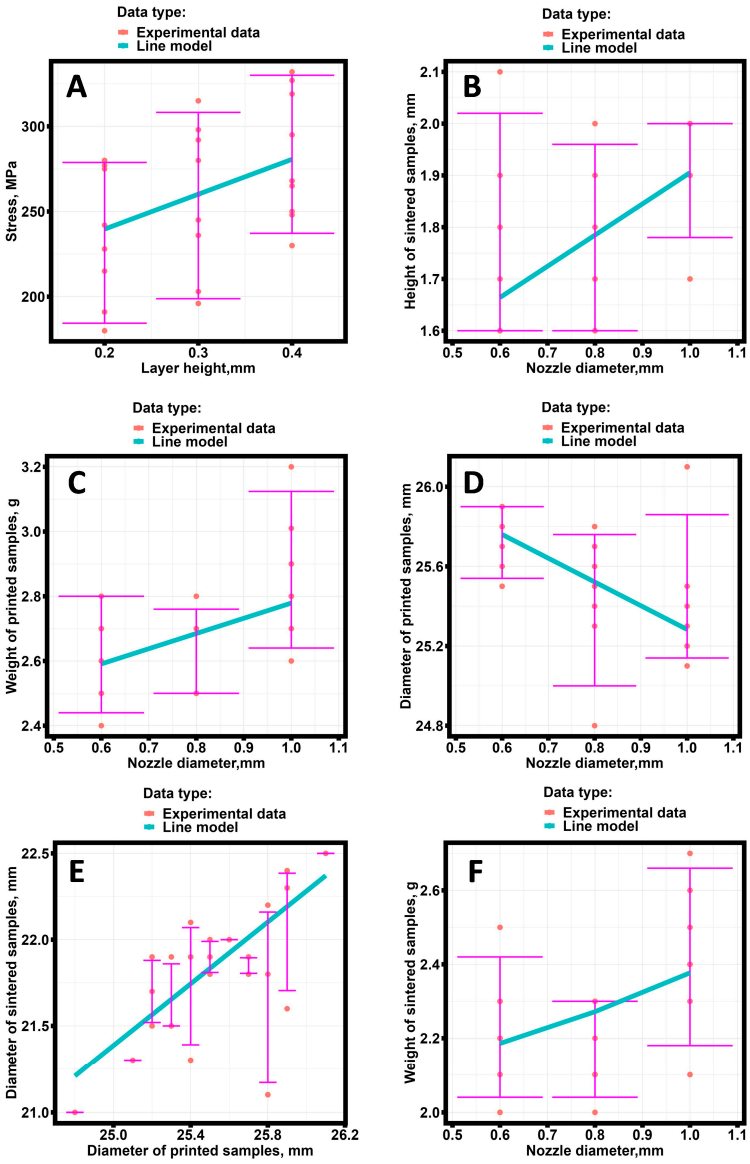

Figure 3. Graphical representation of the identified correlations between flexural strength and nozzle diameter (**A**), sintered specimen thickness and nozzle diameter (**B**), weight of printed samples and nozzle diameter (**C**), diameters of printed samples and nozzle (**D**), diameters of printed and sintered specimens (**E**), thickness of printed and sintered samples (**F**).

In Figure 3F, deviations from the linear relationship are observed. In order to establish the closest mathematical law describing the dependence of the weight of sintered samples on nozzle diameter, four dependencies were considered:

- Linear;
- Parabolic;
- Exponential;
- Logarithmic.

The minimum Akaike criterion was used as the main comparison criterion. As a result of the comparison of dependencies, it was found that the minimum value has an exponential dependence on the form

$$y = a + b \exp(x)$$

A linear equation is given by an equation of the form

$$y = a + b \cdot x$$

where y—dependent variable; x—independent variable; a—the dimension of the studied dependent variable; b—the increment of the dependent variable from the independent variable.

Table 7 presents the linear equations describing the relationship between the correlated parameters.

Table 7. Equations of linear relationships between statistically significantly correlated parameters.

Correlating Parameters		Linear Equations	Mean Square Deviation
σ_H—Layer height (h_l)		$\sigma_H = 198.64 + 205 \cdot h_l$	52.41
Nozzle diameter (d_n)	- w *	$w = 2.31 + 0.47 \cdot d_n$	0.16
	- d *	$d = 26.50–1.19 \cdot d_n$	0.18
	- W	$W = 1.80 + 0.21 \cdot \exp(d_n)$	0.17
	- H	$H = 1.30 + 0.60 \cdot d_n$	0.13
D—d *		$D = -1.00 + 0.90 \cdot d$ *	0.23

* printed samples.

The mean square deviation of the presented robust regression models shows good agreement between the models and the experimental values. Summarizing the results of correlation and regression analysis, it can be concluded that for printing samples from the developed ceramic–polymer filament using FDM technology with subsequent debinding and sintering, the use of a nozzle with a diameter of 0.6 mm and a layer height of 0.4 mm would be optimal. The Kruskal–Wallis test [54] was applied to determine the influence of the filling pattern on the flexural strength of sintered ceramic samples. This method was chosen for values that do not obey the normal law of distribution to determine if there are differences between groups. The results showed that there was no statistically significant effect of filler type on the strength values of ceramic samples (p-value = 0.3908). A similar conclusion was obtained for geometric and weight indices of sintered samples. Summarizing the results of the statistical analysis and taking into account the findings drawn in [34], we can conclude that the distribution of ceramics in the volume of the printed samples is influenced by the layer height and the diameter of the nozzle used in the FDM printer.

4. Conclusions

The application of statistical analysis in the study of the multistage technological process allowed us to establish the presence of implicit linear relationships between nozzle diameter, layer height, and weight of samples printed from 60 vol.% Al_2O_3/40 vol.% PLA

ceramic–polymer filament by FDM technology and characteristics of sintered samples. From the presented results it can be seen that the printed samples with filling type "line" and layer height 0.4 mm have the best mechanical properties. This can be explained by the fact that the fewer horizontal layers in the sample, the fewer voids between them, which negatively affect the mechanical properties. In addition, the greater the line thickness, the fewer horizontal layers need to be extruded to achieve a given disk height, and therefore fewer voids are formed in the printed object. Printing an object with the fill type "line" creates a two-dimensional grid where only one axis is printed along one layer. For the mold sample studied and a density of 100%, this fill type allowed the slicer to place the extruded filaments with as much contact between them as possible, in contrast to the "zigzag" and "concentric" fill patterns. It was found that the flexural strength of the alumina samples increases with increasing layer height of printed specimens. The highest values of the flexural strength were achieved at a layer height equal to 0.4 mm, and the geometric characteristics are closest (the least spread in values) to the model ones when using a nozzle with a diameter of 0.6 mm. Application of the Kruskal–Wallis test showed that there are no statistically significant differences in strength properties and in the change in geometrical parameters of Al_2O_3 samples depending on the filling pattern. The application of Akaike's information criterion combined with robotic regression analysis allowed us to establish the existence of a non-linear relationship between the weight of sintered samples and the nozzle diameter of the nozzle used in the FDM printing of blanks. Generalization of the results obtained in the study allows us to state that geometric parameters of samples and mechanical properties of ceramics are established at the stage of green bodies manufacturing and depend on the equipment parameters and 3D printing conditions. The obtained regularities permit us to optimize the manufacturing process of blanks for subsequent annealing based on the conditions of layer thickness set during printing (setting the strength level) and the need to obtain accurate geometry of the blank (choosing the nozzle diameter). The conducted statistical analysis allows the optimization of the FDM 3D printing parameters of ceramic–polymer samples to obtain ceramic specimens with the required shape and properties. The results of the implementation of the identified statistical regularities will be studied in further works.

Author Contributions: Conceptualization, A.S. and N.N.; data curation, N.W.S.P. and P.P.; formal analysis, E.K. and R.K.; funding acquisition, A.S.; investigation, N.N., R.K. and E.K.; methodology, A.S. and N.N.; project administration, A.S. and N.N.; resources, E.K. and P.P; software, N.N.; N.W.S.P.; supervision, A.S. and N.N.; validation, N.W.S.P. and P.P.; visualization, A.S. and N.N.; writing—original draft, A.S. and N.N. All authors have read and agreed to the published version of the manuscript.

Funding: This work was supported by the Ministry of Science and Higher Education of the Russian Federation under project 0707-2020-0034.

Data Availability Statement: Not applicable.

Acknowledgments: This work was carried on the equipment of the Collective Use Center of MSTU "STANKIN" (project No. 075-15-2021-695).

Conflicts of Interest: The authors declare no conflict of interest.

References

1. Bartolomé, J.F.; Gutiérrez-González, C.F.; Torrecillas, R. Mechanical properties of alumina-zirconia-Nb micro-nano hybrid composites. *Compos. Sci. Technol.* **2007**, *68*, 1392–1398. [CrossRef]
2. Gutiérrez-González, C.F.; Bartolomé, J.F. Damage tolerance and R-curve behaviour of Al_2O_3-ZrO_2-Nb multiphase nanocomposites with synergistic toughening mechanism. *J. Mater. Res.* **2008**, *23*, 570–578. [CrossRef]
3. Rodriguez-Suarez, T.; Bartolomé, J.F.; Smirnov, A.; Lopez-Esteban, S.; Díaz, L.A.; Torrecillas, R.; Moya, J.S. Electroconductive Alumina-TiC-Ni nanonanocomposites obtained by Spark Plasma Sintering. *Ceram. Int.* **2011**, *5*, 1631–1636. [CrossRef]
4. Grigoriev, S.N.; Volosova, M.A.; Peretyagin, P.Y.; Seleznev, A.E.; Okunkova, A.A.; Smirnov, A. The effect of TiC additive on mechanical and electrical properties of Al_2O_3 ceramic. *Appl. Sci.* **2018**, *8*, 2385. [CrossRef]

5. López-Píriz, R.; Goyos-Ball, L.; Cabal, B.; Martínez, S.; Moya, J.S.; Bartolomé, J.F.; Torrecillas, R. New ceramic multi-unit dental abutments with an antimicrobial glassy coating. *Materials* **2022**, *15*, 5422. [CrossRef] [PubMed]
6. Torrecillas, R.; Moya, J.S.; Díaz, L.A.; Bartolomé, J.F.; Fernández, A.; Lopez-Esteban, S. Nanotechnology in joint replacement. *WIREs Nanomed. Nanobiotechnol.* **2009**, *1*, 540–552. [CrossRef]
7. Chevalier, J.; Taddei, P.; Gremillard, L.; Deville, S.; Fantozzi, G.; Bartolomé, J.F.; Pecharro-man, C.; Moya, J.S.; Diaz, L.A.; Torrecillas, R.; et al. Reliability assessment in advanced nanocomposite materials for orthopaedic applications. *J. Mech. Behav. Biomed. Mater.* **2011**, *4*, 303–314. [CrossRef]
8. Jiang, C.-P.; Romario, Y.S.; Toyserkani, E. Development of a Novel Tape-Casting Multi-Slurry 3D Printing Technology to Fabricate the Ceramic/Metal Part. *Materials* **2023**, *16*, 585. [CrossRef]
9. Meshalkin, V.P.; Belyakov, A.V. Methods Used for the Compaction and Molding of Ceramic Matrix Composites Reinforced with Carbon Nanotubes. *Processes* **2020**, *8*, 1004. [CrossRef]
10. Klement, N.; Abdeljaouad, M.A.; Porto, L.; Silva, C. Lot-Sizing and Scheduling for the Plastic Injection Molding Industry—A Hybrid Optimization Approach. *Appl. Sci.* **2021**, *11*, 1202. [CrossRef]
11. Wang, J.; Mao, Q.; Jiang, N.; Chen, J. Effects of Injection Molding Parameters on Properties of Insert-Injection Molded Polypropylene Single-Polymer Composites. *Polymers* **2022**, *14*, 23. [CrossRef] [PubMed]
12. *ISO/ASTM 52900:2015 [ASTM F2792]*; Additive Manufacturing-General Principles-Terminology. International Organization for Standardization ISO: Geneva, Switzerland, 2015.
13. Tosto, C.; Bragaglia, M.; Nanni, F.; Recca, G.; Cicala, G. Fused Filament Fabrication of Alumina/Polymer Filaments for Obtaining Ceramic Parts after Debinding and Sintering Processes. *Materials* **2022**, *15*, 7399. [CrossRef] [PubMed]
14. Nötzel, D.; Eickhoff, R.; Hanemann, T. Fused filament fabrication of small ceramic components. *Materials* **2018**, *11*, 1463. [CrossRef] [PubMed]
15. Iyer, S.; McIntosh, J.; Bandyopadhyay, A.; Langrana, N.; Safari, A.; Danforth, S.C.; Clancy, R.B.; Gasdaska, C.; Whalen, P.J. Microstructural characterization and mechanical properties of Si_3N_4 formed by fused deposition of ceramics. *Int. J. Appl. Ceram. Technol.* **2008**, *5*, 127–137. [CrossRef]
16. Orlovská, M.; Chlup, Z.; Bača, L.; Janek, M.; Kitzmantel, M. Fracture and mechanical properties of lightweight alumina ceramics prepared by fused filament fabrication. *J. Eur. Ceram. Soc.* **2020**, *40*, 4837–4843. [CrossRef]
17. Truxová, V.; Šafka, J.; Sobotka, J.; Macháček, J.; Ackermann, M. Alumina Manufactured by Fused Filament Fabrication: A Comprehensive Study of Mechanical Properties and Porosity. *Polymers* **2022**, *14*, 991. [CrossRef]
18. Schätzlein, E.; Kicker, C.; Söhling, N.; Ritz, U.; Neijhoft, J.; Henrich, D.; Frank, J.; Marzi, I.; Blaeser, A. 3D-Printed PLA-Bioglass Scaffolds with Controllable Calcium Release and MSC Adhesion for Bone Tissue Engineering. *Polymers* **2022**, *14*, 2389. [CrossRef]
19. Elhattab, K.; Bhaduri, S.B.; Sikder, P. Influence of Fused Deposition Modelling Nozzle Temperature on the Rheology and Mechanical Properties of 3D Printed β-Tricalcium Phosphate (TCP)/Polylactic Acid (PLA) Composite. *Polymers* **2022**, *14*, 1222. [CrossRef]
20. Tselikos, G.; Rasul, S.; Groen, P.; Li, C.; Khaliq, J. In Situ Printing and Functionalization of Hybrid Polymer-Ceramic Composites Using a Commercial 3D Printer and Dielectrophoresis—A Novel Conceptual Design. *Polymers* **2021**, *13*, 3979. [CrossRef]
21. Nakonieczny, D.S.; Kern, F.; Dufner, L.; Antonowicz, M.; Matus, K. Alumina and Zirconia-Reinforced Polyamide PA-12 Composites for Biomedical Additive Manufacturing. *Materials* **2021**, *14*, 6201. [CrossRef]
22. Luo, X.; Cheng, H.; Wu, X. Nanomaterials Reinforced Polymer Filament for Fused Deposition Modeling: A State-of-the-Art Review. *Polymers* **2023**, *15*, 2980. [CrossRef]
23. Gonzalez-Gutierrez, J.; Cano, S.; Schuschnigg, S.; Kukla, C.; Sapkota, J.; Holzer, C. Additive Manufacturing of Metallic and Ceramic Components by the Material Extrusion of Highly-Filled Polymers: A Review and Future Perspectives. *Materials* **2018**, *11*, 840. [CrossRef] [PubMed]
24. Baechle-Clayton, M.; Loos, E.; Taheri, M.; Taheri, H. Failures and Flaws in Fused Deposition Modeling (FDM) Additively Manufactured Polymers and Composites. *J. Compos. Sci.* **2022**, *6*, 202. [CrossRef]
25. Chen, Z.; Li, Z.; Li, J.; Liu, C.; Lao, C.; Fu, Y.; Liu, C.; Li, Y.; Wang, P.; He, Y. 3D printing of ceramics. *J. Eur. Ceram. Soc.* **2019**, *39*, 661–687. [CrossRef]
26. Doshi, M.; Mahale, A.; Kumar Singh, S.; Deshmukh, S. Printing parameters and materials affecting mechanical properties of FDM-3D printed Parts: Perspective and prospects. *Mater. Today Proc.* **2022**, *50*, 2269–2275. [CrossRef]
27. Tsung, F.; Li, Y.; Jin, M. Statistical Process Control for Multistage Manufacturing and Service Operations: A Review. In Proceedings of the 2006 IEEE International Conference on Service Operations and Logistics, and Informatics, Shanghai, China, 21–23 June 2006; pp. 752–757.
28. Banker, R.; Kotarac, K.; Neralić, L. Sensitivity and stability in stochastic data envelopment analysis. *J. Oper. Res. Soc.* **2015**, *66*, 134–147. [CrossRef]
29. Fountas, N.A.; Zaoutsos, S.; Chaidas, D.; Kechagias, J.D.; Vaxevanidis, N.M. Statistical modelling and optimization of mechanical properties for PLA and PLA/Wood FDM materials. *Mater. Today Proc.* 2023, in press. [CrossRef]
30. Banerjee, D.; Mishra, S.B.; Khan, M.S.; Kumar, M.A. Mathematical approach for the geometrical deformation of fused deposition modelling build parts. *Mater. Today Proc.* **2020**, *33*, 5051–5054. [CrossRef]

31. Fountas, N.A.; Kostazos, P.; Pavlidis, H.; Antoniou, V.; Manolakos, D.E.; Vaxevanidis, N.M. Experimental investigation and statistical modelling for assessing the tensile properties of FDM fabricated parts. *Procedia Struct. Integr.* **2020**, *26*, 139–146. [CrossRef]
32. Crockett, R.S.; Calvert, P.D. The liquid-to-solid transition in stereodeposition techniques. In *Solid Freeform Fabrication Proceedings*; The University of Arizona: Tucson, AZ, USA, 1996; pp. 257–264.
33. Anitha, R.; Arunachalam, S.; Radhakrishan, P. Critical parameters influencing the quality if prototypes in fused deposition modeling. *J. Mater. Process. Technol.* **2001**, *118*, 385–388. [CrossRef]
34. Bellini, A.; Güçeri, S.; Bertoldi, M. Liquefier dynamics in fused deposition. *J. Manuf. Sci. Eng Trans.* **2004**, *126*, 237–246. [CrossRef]
35. Venkataraman, N.; Rangarajan, S.; Matthewson, M.J.; Harper, B.; Safari, A.; Danforth, S.C.; Wu, G.; Langrana, N.; Guceri, S.; Yardimci, A. Feedstock material property-process relationships in fused deposition of ceramics (FDC). *Rapid Prototyp. J.* **2002**, *6*, 244–252. [CrossRef]
36. Venkataraman, N.; Rangarajan, S.; Matthewson, M.J.; Safari, A.; Danforth, S.C.; Yardimci, A. Mechanical and rheological properties of feedstock material for fused deposition of ceramics and metals (FDC and FDMet) and their relationship to process performance. In *Solid Freeform Fabrication Proceedings*; University of Texas Libraries: Austin, TX, USA, 1999; pp. 351–360.
37. Beloglazov, I.; Krylov, K. An Interval-Simplex Approach to Determine Technological Parameters from Experimental Data. *Mathematics* **2022**, *10*, 2959. [CrossRef]
38. Chatfield, C. *Statistics for Technology: A Course in Applied Statistics*; Routledge: Oxford, UK, 2018.
39. Melcher, J.; Kala, Z.; Holický, M.; Fajkus, M.; Rozlívka, L. Design characteristics of structural steels based on statistical analysis of metallurgical products. *J. Construct. Steel Res.* **2004**, *60*, 795–808. [CrossRef]
40. Kontopantelis, E.; Reeves, D. Performance of statistical methods for meta-analysis when true study effects are non-normally distributed: A simulation study. *Stat. Methods Med. Res.* **2010**, *21*, 409–426. [CrossRef] [PubMed]
41. Skorodumov, S.V.; Neganov, D.A.; Studenov, E.P.; Poshibaev, P.V.; Nikitin, N.Y. Statistical analysis of mechanical test results for samples of pipes from trunk oil pipelines after long-term operation. Industr. *Lab. Diagn. Mater.* **2022**, *88*, 82–91. [CrossRef]
42. *ISO 6872:2019*; Dentistry—Ceramic materials. International Organization for Standardization ISO: Geneva, Switzerland, 2019.
43. Huang, C.W.; Hsueh, C.H. Piston-on-three-ball versus piston-on-ring in evaluating the biaxial strength of dental ceramics. *Dent. Mater.* **2011**, *27*, 117–123. [CrossRef]
44. Smirnov, A.; Beltrán, J.I.; Rodriguez-Suarez, T.; Pecharromán, C.; Muñoz, M.C.; Moya, J.S.; Bartolomé, J.F. Unprecedented simultaneous enhancement in damage tolerance and fatigue resistance of zirconia/Ta composites. *Sci. Rep.* **2017**, *21*, 44922. [CrossRef] [PubMed]
45. Smirnov, A.; Kurland, H.-D.; Grabow, J.; Müller, F.A.; Bartolomé, J.F. Microstructure, mechanical properties and low temperature degradation resistance of 2Y-TZP ceramic materials derived from nanopowders prepared by laser vaporization. *J. Eur. Ceram. Soc.* **2015**, *35*, 2685–2691. [CrossRef]
46. Shetty, D.K.; Rosenfield, A.R.; Mcguire, P.; Bansal, G.K.; Duckworth, W.H. Biaxial Flexure Test for Ceramics. *J. Am. Ceram. Soc.* **1980**, *59*, 1193–1197.
47. Smirnov, A.; Terekhina, S.; Tarasova, T.; Hattali, L.; Grigoriev, S. From the development of low-cost flament to 3D printing ceramic parts obtained by fused filament fabrication. *Int. J. Adv. Manuf. Technol.* **2023**, *128*, 511–529. [CrossRef]
48. Nötzel, D.; Hanemann, T. New Feedstock System for Fused Filament Fabrication of Sintered Alumina Parts. *Materials* **2020**, *13*, 4461. [CrossRef]
49. Dufour, J.M.; Farhat, A.; Gardiol, L.; Khalaf, L. Simulation-based finite sample normality tests in linear regressions. *Econom. J.* **1998**, *1*, 154–173. [CrossRef]
50. Shapiro, S.S.; Wilk, M.B. An analysis of variance test for normality. *Biom. Trust* **1965**, *52*, 591–611. [CrossRef]
51. Kolmogorov, A.N. Sulla determinazione empirica di une legge di distribuzione. *G. Ist. Ital. Attuari* **1933**, *4*, 83–91.
52. Venables, W.N.; Ripley, B.D. *Modern Applied Statistics with S*; Springer: New York, NY, USA, 2002; pp. 435–446.
53. Smirnov, A.; Peretyagin, P.; Nikitin, N. Assessment effect of nanometer-sized Al_2O_3 fillers in polylactide on fracture probability of filament and 3D printed samples by FDM. *Materials* **2023**, *16*, 1671. [CrossRef]
54. Kruskal, W.H.; Wallis, W.A. Use of ranks in one-criterion variance analysis. *J. Am. Stat. Assoc.* **1952**, *47*, 583–621. [CrossRef]